Journal of Applied Physics

Carbon-nanotube-templated carbon nanofibers with improved mechanical performance

Cite as: J. Appl. Phys. **129**, 044303 (2021); https://doi.org/10.1063/5.0031159
Submitted: 28 September 2020 • Accepted: 06 January 2021 • Published Online: 22 January 2021

Wei Zhao, Yongqiang Zhang, Xiaoguang Wang, et al.

Journal of Applied Physics ARTICLE scitation.org/journal/jap

Carbon-nanotube-templated carbon nanofibers with improved mechanical performance

Cite as: J. Appl. Phys. **129**, 044303 (2021); doi: 10.1063/5.0031159
Submitted: 28 September 2020 · Accepted: 6 January 2021 ·
Published Online: 22 January 2021

View Online Export Citation CrossMark

Wei Zhao,[1,2] Yongqiang Zhang,[3] Xiaoguang Wang,[3] Huanhuan Lu,[3] Guozhu Liu,[2] Jinghe Wei,[2] Zhiwei Shan,[3,a)] Peng Liu,[1,a)] Kaili Jiang,[1,a)] and Shoushan Fan[1]

AFFILIATIONS

[1]State Key Laboratory of Low-Dimensional Quantum Physics, Department of Physics and Tsinghua-Foxconn Nanotechnology Research Center, Tsinghua University, Beijing 100084, China
[2]The 58th Research Institute of China Electronics Technology Group Corporation, Wuxi, Jiangsu 214035, China
[3]Center for Advancing Materials Performance from the Nanoscale (CAMP-Nano) and Hysitron Applied Research Center in China (HARCC), State Key Laboratory for Mechanical Behavior of Materials, Xi'an Jiaotong University, Xi'an 710049, China

Note: This paper is part of the Special Topic on Physics and Applications of Nanotubes.
[a)]**Authors to whom correspondence should be addressed:** zwshan@mail.xjtu.edu.cn; pengliu@tsinghua.edu.cn; and JiangKL@tsinghua.edu.cn

ABSTRACT

The carbon nanotube (CNT) is a compelling and promising material for industrial applications requiring high strength and rigidity. For a multi-walled CNT (MWCNT), the nominal tensile strength and Young's modulus (considering the whole cross-sectional area of the specimen) are key mechanical factors for the practical application of macroscopic fibers and composites. However, the nominal tensile strength and Young's modulus of MWCNTs are much lower than their effective tensile strength and Young's modulus (considering the fracture cross-sectional area) because the outermost graphite layer always fractures first due to the low cross-link between graphite layers. In this paper, we fabricated the carbon nanofibers (CNFs) by epitaxial growth on super-aligned MWCNT film template and conducted *in situ* uniaxial tensile tests on individual carbon-nanotube-templated CNFs. The individual CNFs show improved nominal mechanical performance than previously reported MWCNTs. The nominal mechanical properties enhancement of the CNFs is attributed to the effective control on load transfer between interwalls.

I. INTRODUCTION

The carbon nanotube (CNT) is an allotrope of carbon with a cylindrical nanostructure, which exhibits extraordinary mechanical performance.[1–10] For industrial production and application of CNTs, the nominal tensile strength and Young's modulus (considering the whole cross-sectional area of the specimen) of a CNT are more important and practical physical quantities than the effective tensile strength and Young's modulus (considering the fracture cross-sectional area of the specimen). Unfortunately, for a multi-walled CNT (MWCNT), there is a tendency that an MWCNT of larger diameter shows lower nominal tensile strength and lower nominal Young's modulus.[6,8,11] These lower values occur because only the outermost graphite layer of the MWCNT fractures first. Recently, the additive synthesis of continuous, aligned, catalyst-free carbon nanofiber (CNF) film from a super-aligned MWCNT (SA-MWCNT) film template has been reported.[12] However, the properties of individual carbon-nanotube-templated CNFs have not been investigated. In this paper, we extracted individual CNFs from the CNF film and measured the nominal tensile strength and Young's modulus of the individual CNFs by *in situ* uniaxial tensile tests inside a transmission electron microscope (TEM). Two types of CNFs, the pristine CNFs (P-CNFs) and the graphitized CNFs (G-CNFs), have been tested. Although the carbon-nanotube-templated CNFs have larger diameters than MWCNTs, the CNFs show improved nominal mechanical performance than previously reported MWCNTs. We attribute the excellent nominal mechanical properties of CNFs to the effective control on load transfer between interwalls, which results in a multi-wall fracture in tensile tests.

II. EXPERIMENTAL

The P-CNF film was synthesized by depositing pyrolytic carbon on the SA-MWCNT film, which served as a template.[12] The thickness of the epitaxial pyrolytic carbon layer, from nanometers to micrometers, can be controlled by adjusting the deposition conditions. After that, each fiber in the film has an "annual ring" cross section, with an MWCNT core and a graphitic periphery, indicating the MWCNT's function as a template.[12] Considering the applications requiring good electrical conductivity and good thermal conductivity, the P-CNF film can be graphitized at high temperature (2900 °C), which is denoted as the G-CNF film.[12] Figures 1(a) and 1(b) show the TEM images of P-CNF and G-CNF, respectively. For the G-CNF, the absence of a distinct interface between the MWCNT template (diameter ∼10 nm) and the graphitic periphery implies an epitaxial growth mechanism of the CNF.[12] Raman spectra of the P-CNF film and the G-CNF film are shown in Figs. 1(c) and 1(d), respectively. The Raman intensity ratios (I_G/I_D) of the P-CNF and the G-CNF are 1.4 and 15.7, respectively, suggesting that the graphitization degree of the G-CNF is much higher than that of the P-CNF.[13]

An individual P-CNF or G-CNF was transferred to a push-to-pull (PTP) device (developed by Hysitron, Inc.) using an Omniprobe micromanipulator in an FEI dual-beam focused ion beam (FIB)/scanning electron microscope (SEM) system [Figs. 2(a) and 2(b)], with the method similar to the one reported in the previous literature.[14–18] As shown in Fig. 2(b), the CNF is bridging the specimen gap of the PTP device, and two platinum (Pt) patches were deposited at the two ends of the fiber to firmly bond the CNF on the PTP device.

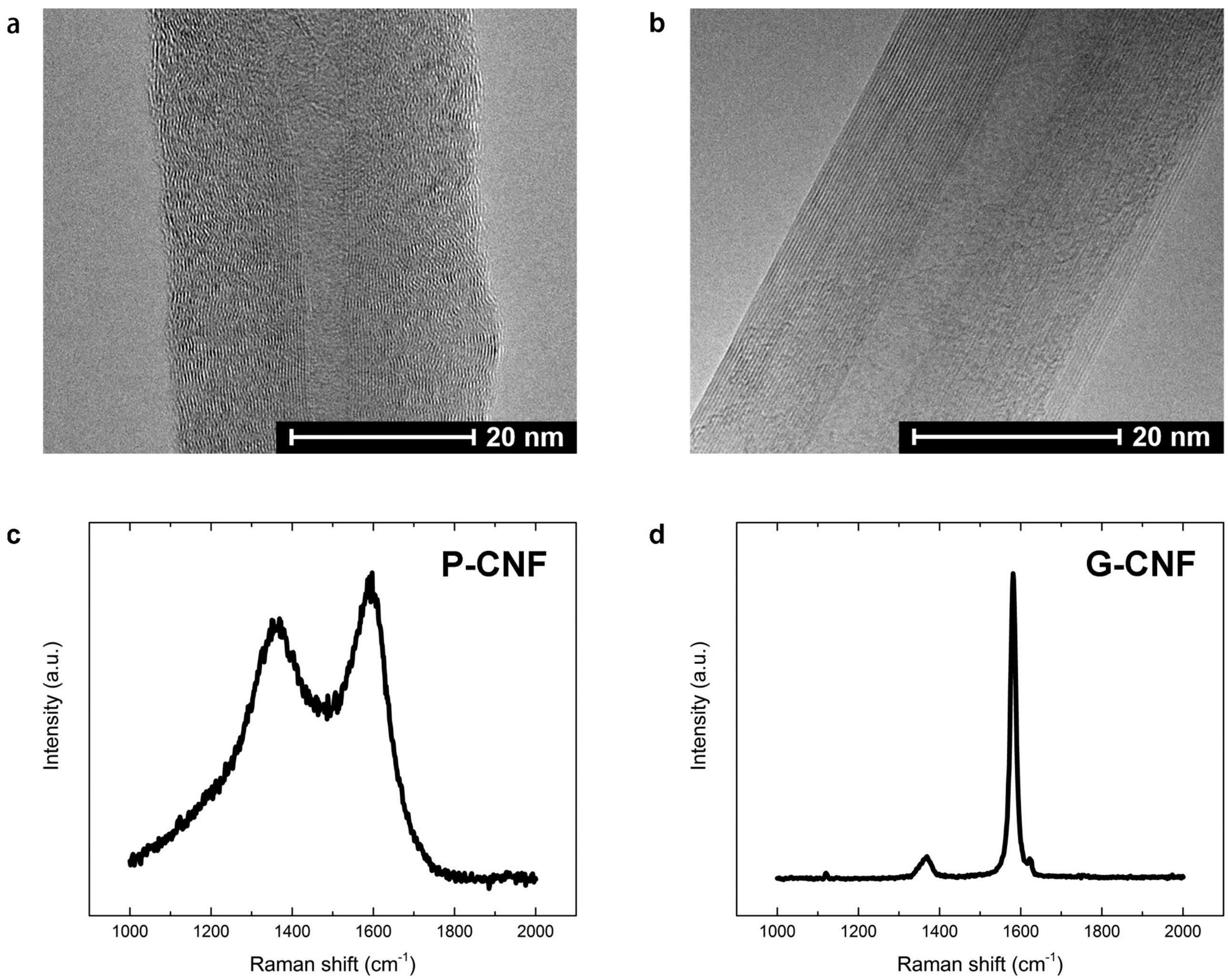

FIG. 1. Characterization of the pristine carbon nanofiber (P-CNF) and the graphitized carbon nanofiber (G-CNF). (a) Transmission electron microscopy (TEM) image of an individual P-CNF. (b) TEM image of an individual G-CNF. (c) Raman spectrum of the P-CNF film. (d) Raman spectrum of the G-CNF film.

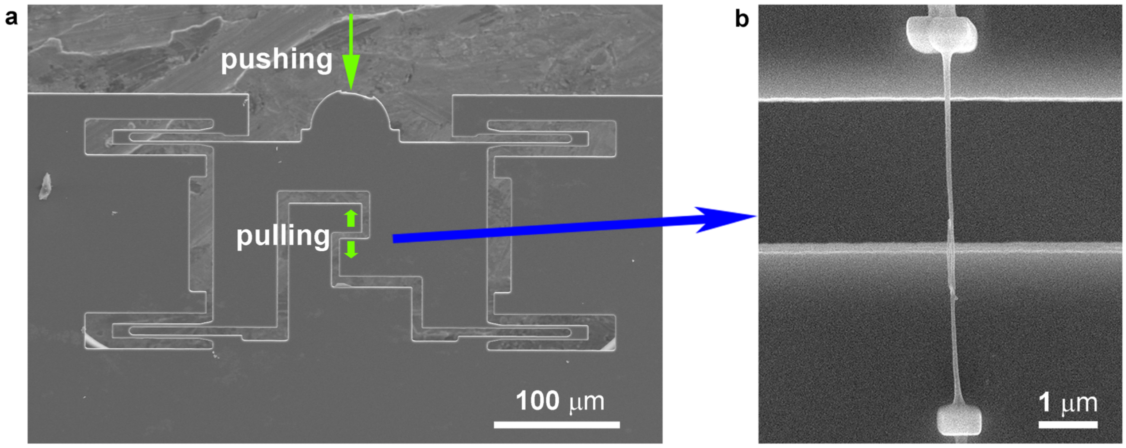

FIG. 2. *In situ* uniaxial tensile test of individual CNFs. (a) Scanning electron microscopy (SEM) image of a PTP device. (b) Magnified SEM image of a CNF sample bridging the sample gap of the PTP device.

The *in situ* tensile tests were realized by a TEM nanoindentation device (PI 95 PicoIndenter from Hysitron, Inc., Minneapolis, MN, USA) coupled with the PTP device. The test method was introduced in detail in the previous literature.[14,18] The P-CNF or G-CNF sample was pulled uniaxially in tension, attenuated by the PTP device [Figs. 2(a) and 2(b)]. The stiffness values of PTP devices, ranging from 151 N/m to 452 N/m, can be calculated by the tensile test without samples. After subtracting the mechanical response of the PTP device, the nominal (considering the whole cross-sectional area of the CNF, including the inner hole of the MWCNT template) stress–strain behavior of the P-CNF and the G-CNF sample could be obtained (for details, see the supplementary material).

III. RESULTS AND DISCUSSION

Figures 3(a)–3(d) show the TEM images of P-CNF and G-CNF and their corresponding nominal stress–strain curves. The nominal stress–strain curves of P-CNF and G-CNF are quite linear before fracture, indicating that the CNF samples are stretched in the elastic region. The (0001) diffraction spots of the G-CNF as shown in Fig. 3(c) indicate that the graphitization degree of the G-CNF sample is much higher than that of the P-CNF as shown in Fig. 3(a).

We conducted tensile tests of three P-CNF samples and four G-CNF samples. The measured fracture strains of G-CNFs ranged from 1.1% to 2.8%. In contrast, the measured fracture strains of P-CNFs ranged from 2.0% to 4.8%, exhibiting higher values than G-CNFs. A more significant difference between P-CNF and G-CNF is that the P-CNF fractures in the "clean break" mode, while the G-CNF fractures in the "sword in sheath" mode. For P-CNF, the "clean break" mode means that the MWCNT core and the graphitic periphery fractured simultaneously [Figs. 4(a) and 4(b)]. In contrast, Figs. 4(c) and 4(d) show a fractured G-CNF, exhibiting that the graphitic periphery fractured before the MWCNT core fractured. In this test, the MWCNT core acted as a sword and the graphitic periphery acted as a sheath, while Fig. S1 in the supplementary material shows two examples of "sword in sheath" fractured G-CNFs that are slightly different from the fractured G-CNF as shown in Figs. 4(c) and 4(d) (for details, see the supplementary material). The different fracture modes of P-CNF and G-CNF result from the graphitization process. For P-CNF, the graphitization degree is low, so the cross-link interaction between graphite results in a good load transfer from the outer walls to the inner ones, and thus a "clean break" fracture [Fig. 4(e)]. For G-CNF, the graphitization degree is high, and the graphite layers are almost perfectly aligned with the axis of the MWCNT core [Fig. 4(f)], which results in a weaker interwall load transfer than that of P-CNF, and thus a "sword in sheath" fracture.

We calculated the nominal tensile strength and Young's modulus according to the whole cross-sectional area of the specimen, including the inner hole of the MWCNT template. These mechanical parameters are better suited for industrial applications. Previous tensile tests of MWCNTs showed that the MWCNT tended to fracture in the "sword in sheath" mode.[6,8,11] Usually, only the outermost graphite layer of MWCNT fractured. The fracture cross-sectional ratio that can be calculated by the fractured cross-sectional area divided by the whole cross-sectional area was much lower than 1. Thus, the nominal tensile strength and Young's modulus of MWCNT are much lower than their effective tensile strength and Young's modulus as reported in Refs. 6, 8, and 11. We calculated nominal tensile strength and Young's modulus of the previously reported MWCNTs based on the data of outer diameter and breaking force provided in the original papers (for details, see Refs. 6, 8, and 11). Figures 5(a) and 5(b) show the comparison of previous results of MWCNTs[6,8,11] and the test results of CNFs. It can be observed that in each study of MWCNTs, the thicker MWCNTs tend to exhibit much lower nominal tensile strengths and Young's moduli than the thinner ones. This sharp reduction results from the fracture mechanism in which only the outermost graphite layer of MWCNT fractures in the tensile test.

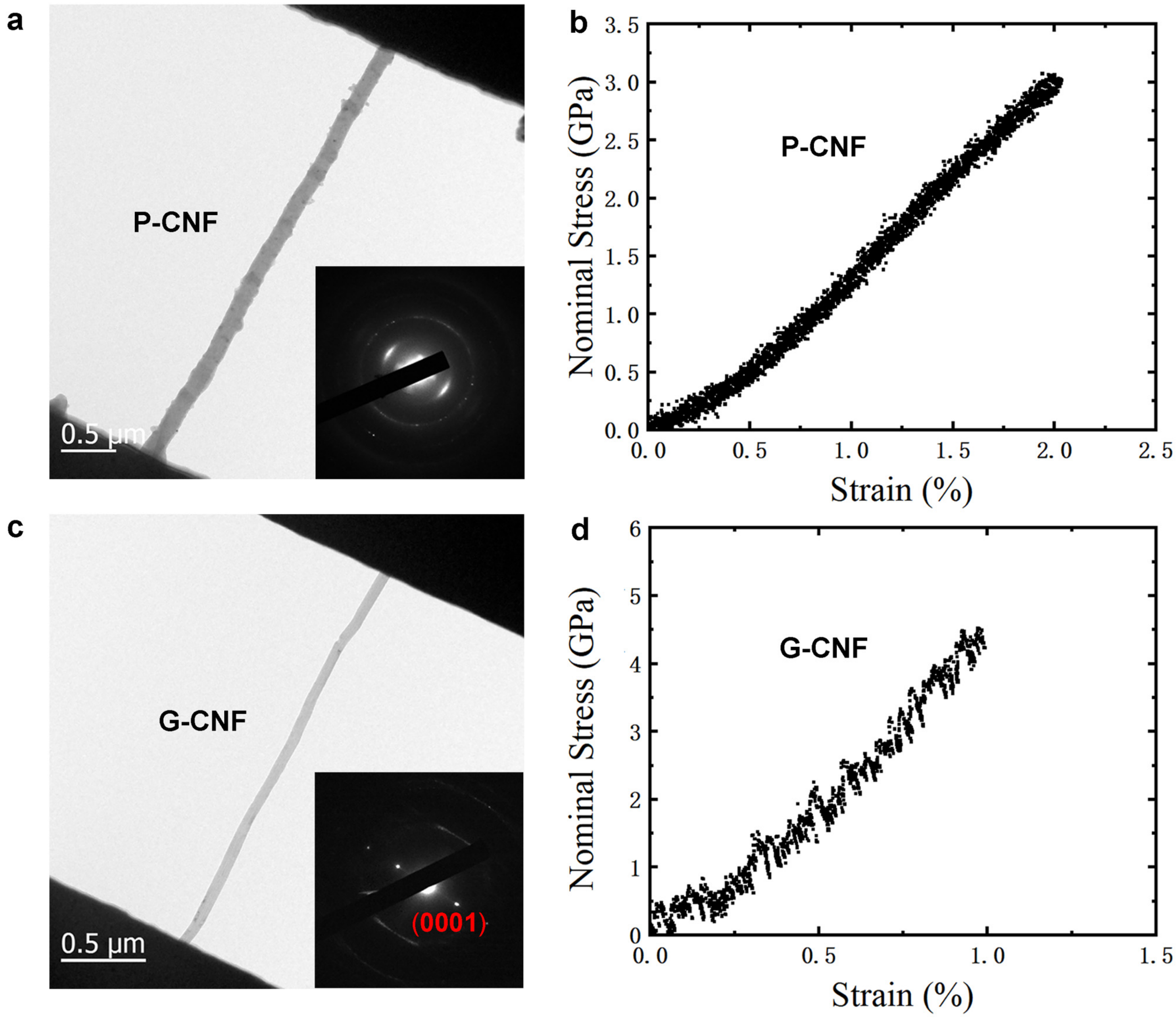

FIG. 3. Tensile tests of P-CNF and G-CNF. (a) TEM image of a P-CNF sample on a PTP device. Inset is the selected-area electron diffraction (SAED) pattern of the P-CNF sample. (b) Nominal stress–strain curve of the P-CNF sample as shown in (a). (c) TEM image of a G-CNF sample on a PTP device. Inset is the SAED pattern of the G-CNF sample. The (0001) diffraction spots are marked. (d) Nominal stress–strain curve of the G-CNF sample as shown in (c).

In contrast, although the diameters of G-CNFs are significantly larger than those of MWCNTs, the nominal tensile strengths of G-CNFs are comparable to those of thinner MWCNTs, and the nominal Young's moduli are much higher than those of thinner MWCNTs. We attribute the high nominal tensile strength and Young's modulus of G-CNF to appropriate cross-link interaction between adjacent graphite layers, which permits an effective load transfer between interwalls, resulting in the fracture of more graphite layers than MWCNT.

It was reported that after a 2600 °C annealing process, chemical vapor deposition (CVD)-grown MWCNTs showed lower nominal tensile strength and Young's modulus than those underwent the 2200 °C annealing process, due to a weaker interwall load transfer.[10] In contrast, even though the G-CNF film was graphitized under 2900 °C, the G-CNF shows high nominal tensile strength and Young's modulus, indicating an effective interwall load transfer. Since the graphitization degree of the P-CNF is much lower than the pristine CVD-grown MWCNT, high-temperature graphitization of P-CNF not only reduces the defect density of graphite layers but also preserves the cross-link interaction between graphite layers. By adjusting the graphitization parameter, we may find an optimal G-CNF structure of higher nominal tensile strength and Young's

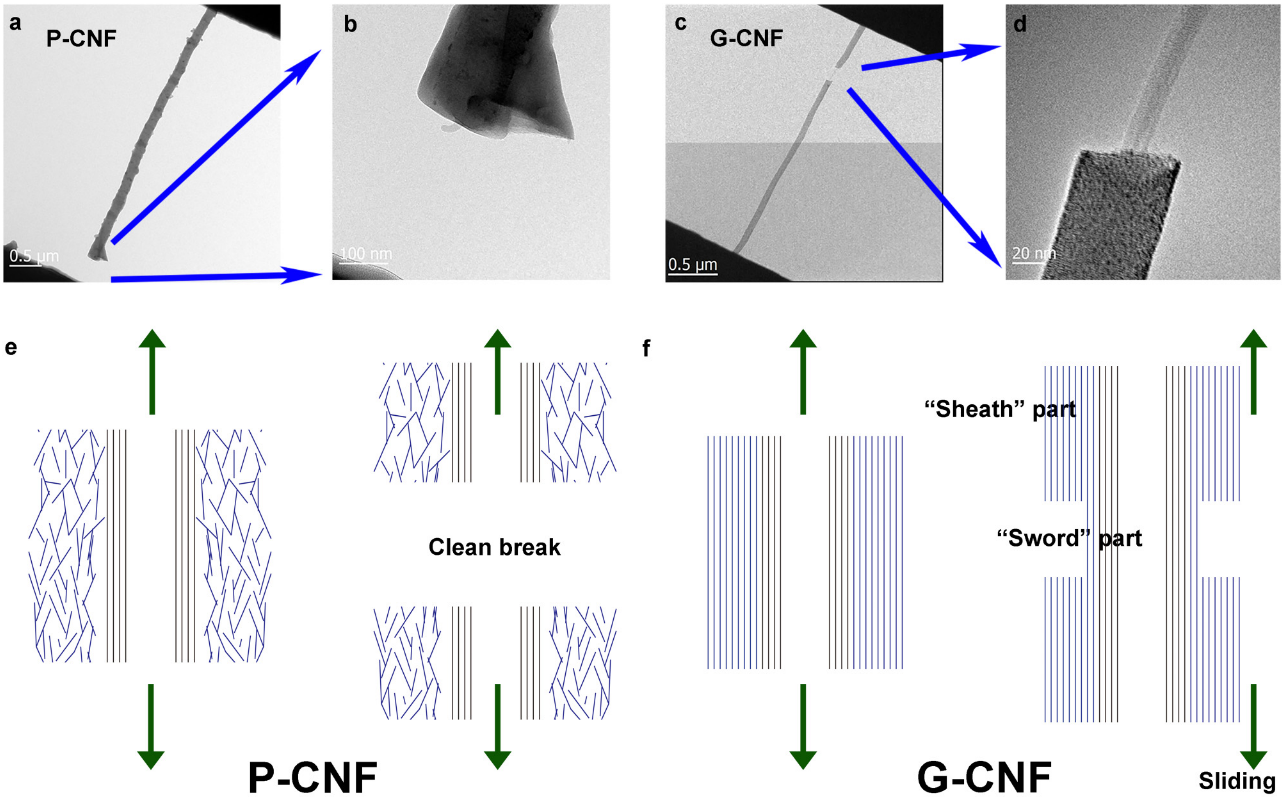

FIG. 4. Characterization of the fracture modes of P-CNF and G-CNF. (a) TEM image of a fractured P-CNF after the tensile test. (b) High-magnification TEM image of the fractured P-CNF, as shown in (a). (c) TEM image of a fractured G-CNF after the tensile test. (d) High-magnification TEM image of the fractured G-CNF, as shown in (c). (e) Schematic of the "clean break" fracture mode of P-CNF. (f) Schematic of the "sword in sheath" fracture mode of G-CNF. The black lines in (e) and (f) indicate the MWCNT core. The blue lines in (e) and (f) indicate the graphitic periphery.

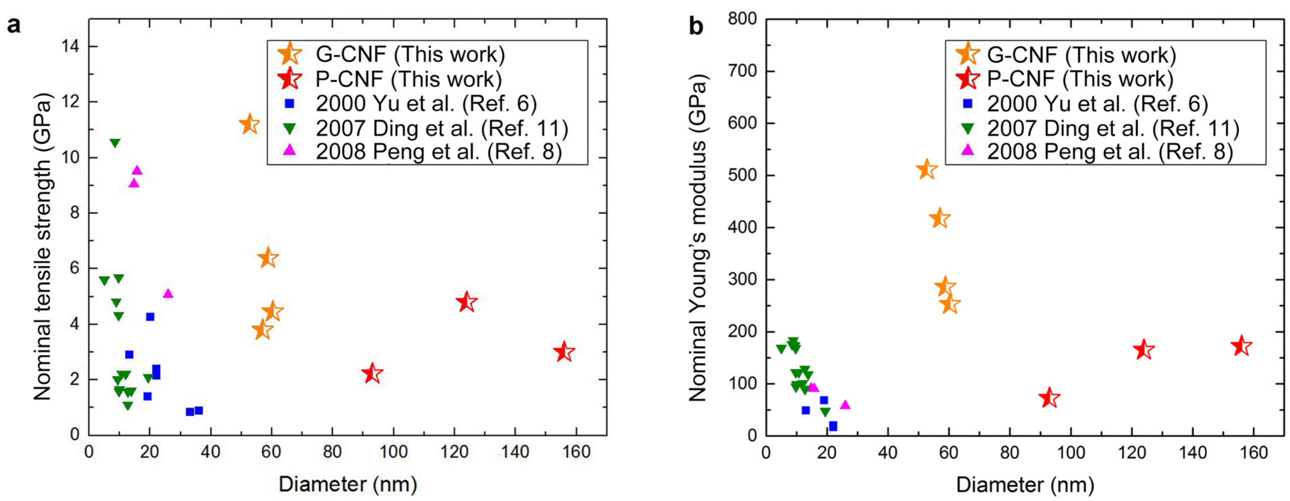

FIG. 5. Comparisons of P-CNFs, G-CNFs, and previously reported MWCNTs (Refs. 6, 8, and 11) with respect to their nominal tensile strength and Young's modulus. (a) Comparison of nominal tensile strength between CNFs and previously reported MWCNTs. (b) Comparison of nominal Young's modulus between CNFs and previously reported MWCNTs.

modulus; not too weak but also not too strong interwall coupling to permit an adequate load transfer between graphite layers, and thus a consequent "clean break" fracture.[19] When comparing P-CNF and the previously reported MWCNTs, the nominal tensile strengths and Young's moduli of P-CNFs are comparable to those of MWCNTs. Since the nominal tensile strength and Young's modulus of the carbon fiber reduced along with the increase in diameter,[20–23] the G-CNF and the P-CNF may exhibit better mechanical performance if we deposit thinner pyrolytic carbon on the SA-MWCNT template.

IV. CONCLUSION

In conclusion, we conducted tensile tests of individual carbon-nanotube-templated CNFs, including P-CNFs and G-CNFs. Although the individual CNFs tested have larger diameters than the SA-MWCNT template, the G-CNFs and P-CNFs show improved nominal mechanical performance than previously reported MWCNTs. The nominal mechanical properties enhancement of the P-CNFs and the G-CNFs is attributed to the effective control on load transfer between interwalls, which leads to a multiwall fracture in tensile tests. For G-CNFs, we may find an optimal CNF structure of higher nominal tensile strength and Young's modulus by adjusting the graphitization parameter; not too weak but also not too strong interwall coupling to permit an adequate load transfer between graphite layers, and thus a consequent "clean break" fracture mode instead of the "sword in sheath" fracture mode. We hope that our experimental results will help improve the quality of CNF films. Since P-CNF films can be continuously fabricated from SA-MWCNT films and G-CNF films exhibit good electrical conductivity and good thermal conductivity, we expect a large-scale application of CNFs in the field requiring high mechanical performance, good electrical conductivity, and good thermal conductivity.

SUPPLEMENTARY MATERIAL

See the supplementary material for TEM characterization of two fractured G-CNF samples (Note S1), TEM images of two fractured G-CNF samples (Fig. S1), nominal stress–strain curves of four G-CNFs and three P-CNFs (Fig. S2), and tensile test results of G-CNFs and P-CNFs (Table S1).

AUTHORS' CONTRIBUTIONS

W.Z., Y.Z., and X.W. contributed equally to this work.

ACKNOWLEDGMENTS

This work was financially supported by the National Key Research and Development Program of China (Nos. 2018YFA0208401 and 2017YFA0205800) and the National Natural Science Foundation of China (NNSFC) (Nos. 51727805, 51672152, 51788104, and 51231005). This work was supported in part by the Beijing Advanced Innovation Center for Future Chip (ICFC). Z. Shan and his students acknowledge the support of the National Key Research and Development Program of China (No. 2017YFB0702001), NNSFC (No. 51621063), and Basic Science Research in Shan Xi (No. 2015JQ5164). We also appreciate the support from the International Joint Laboratory for Micro/Nano Manufacturing and Measurement Technologies and the Collaborative Innovation Center of High-End Manufacturing Equipment. The authors thank Professor Wei Xianlong and Dr. Tang Zhiqiang for their valuable help during the sample preparation.

DATA AVAILABILITY

The data that support the findings of this study are available from the corresponding author upon reasonable request.

REFERENCES

1. M. J. Treacy, T. Ebbesen, and J. Gibson, Nature **381**, 678 (1996).
2. J. P. Lu, Phys. Rev. Lett. **79**, 1297 (1997).
3. E. W. Wong, P. E. Sheehan, and C. M. Lieber, Science **277**, 1971 (1997).
4. J. P. Salvetat, G. A. D. Briggs, J. M. Bonard, R. R. Bacsa, A. J. Kulik, T. Stöckli, N. A. Burnham, and L. Forró, Phys. Rev. Lett. **82**, 944 (1999).
5. P. Poncharal, Z. L. Wang, D. Ugarte, and W. A. De Heer, Science **283**, 1513 (1999).
6. M. F. Yu, O. Lourie, M. J. Dyer, K. Moloni, T. F. Kelly, and R. S. Ruoff, Science **287**, 637 (2000).
7. M. F. Yu, B. S. Files, S. Arepalli, and R. S. Ruoff, Phys. Rev. Lett. **84**, 5552 (2000).
8. B. Peng, M. Locascio, P. Zapol, S. Li, S. L. Mielke, G. C. Schatz, and H. D. Espinosa, Nat. Nanotechnol. **3**, 626 (2008).
9. T. Filleter, R. Bernal, S. Li, and H. D. Espinosa, Adv. Mater. **23**, 2855 (2011).
10. G. Yamamoto, K. Shirasu, Y. Nozaka, Y. Sato, T. Takagi, and T. Hashida, Carbon **66**, 219 (2014).
11. W. Ding, L. Calabri, K. Kohlhaas, X. Chen, D. Dikin, and R. S. Ruoff, Exp. Mech. **47**, 25 (2007).
12. X. Lin, W. Zhao, W. Zhou, P. Liu, S. Luo, H. Wei, G. Yang, J. Yang, J. Cui, and R. Yu, ACS Nano **11**, 1257 (2017).
13. A. C. Ferrari, Solid State Commun. **143**, 47 (2007).
14. H. Guo, K. Chen, Y. Oh, K. Wang, C. Dejoie, S. A. Syed Asif, O. L. Warren, Z. W. Shan, J. Wu, and A. M. Minor, Nano Lett. **11**, 3207 (2011).
15. Y. Oh, E. Cyrankowski, Z. Shan, and S. A. Syed Asif, U.S. patent 008434370B2 (7 May 2013).
16. Y. Oh, E. Cyrankowski, Z. Shan, and S. A. Syed Asif, U.S. patent 008789425B2 (29 July 2014).
17. S. Dai, J. Zhao, M. He, X. Wang, J. Wan, Z. Shan, and J. Zhu, Nano Lett. **15**, 8 (2015).
18. X. Wang, K. Chen, Y. Zhang, J. Wan, O. L. Warren, J. Oh, J. Li, E. Ma, and Z. Shan, Nano Lett. **15**, 7886 (2015).
19. K. Shirasu, I. Tamaki, T. Miyazaki, G. Yamomoto, R. Bekarevich, K. Hirahara, Y. Shimamura, Y. Inoue, and T. Hashida, Mech. Eng. J. **4**, 17-00029 (2017).
20. G. Tibbetts and C. Beetz, Jr., J. Phys. Appl. Phys. **20**, 292 (1987).
21. G. Tibbetts, *Carbon Fibers, Filaments and Composites* (Springer, Dordrecht, 1990), pp. 73–94.
22. T. Tagawa and T. Miyata, Mater. Sci. Eng. A **238**, 336 (1997).
23. A. M. Beese, D. Papkov, S. Li, Y. Dzenis, and H. D. Espinosa, Carbon **60**, 246 (2013).